Liquid–Liquid Equilibria of Dipropylene Glycol Dimethyl Ether and Water by Molecular Dynamics

Thorsten Köddermann[a], Karl N. Kirschner[a], Jadran Vrabec[b], Marco Hülsmann[a], Dirk Reith[*,a]

[a] *Fraunhofer-Institut für Algorithmen und Wissenschaftliches Rechnen (SCAI), Schloss Birlinghoven, 53754 Sankt Augustin, Germany*

[b] *Lehrstuhl für Thermodynamik und Energietechnik (ThEt), Universität Paderborn, Warburger Str. 100, 33098 Paderborn, Germany*

Abstract

In the framework of the Industrial Fluid Properties Simulation Challenge 2010, liquid–liquid equilibria of dipropylene glycol dimethyl ether and water are determined by molecular dynamics simulation. A new force field for the ether was developed and combined with a water model from the literature (TIP4P/2005). According to the specifications of the competition, molar fractions of the components in the coexisting phases are predicted over a temperature range from 283 to 353 K.

Key words: Liquid–Liquid Equilibria, Ether, Water, Force Field Parameterization, Molecular Dynamics

1. Introduction

The Industrial Fluid Property Simulation Challenge (IFPSC) 2010 is devoted to "test the ability of computer modeling to predict the mutual solubility in liquid–liquid equilibria (LLE) of water and a glycol ether as a function of temperature" [1]. The compound of interest is dipropylene glycol dimethyl ether (DPGDME, $C_8H_{18}O_3$) with the CAS number 111109-77-4 and the EINECS number 404-640-5. E.g., it is sold under the trademark "Proglyde DMM" by Dow Chemical or under its chemical name by Merck Chemicals (Germany) or by Shuyang Hengrun Fine Chemical Co. (China). DPGDME is a mixture of the following three isomers

- CH_3-O-CH(CH_3)-CH_2-O-CH_2-CH(CH_3)-O-CH_3 (isomer I, CAS number 63019-84-1),
- CH_3-O-CH(CH_3)-CH_2-O-CH(CH_3)-CH_2-O-CH_3 (isomer II, CAS number 89399-28-0),
- CH_3-O-CH_2-CH(CH_3)-O-CH(CH_3)-CH_2-O-CH_3 (isomer III, no CAS number),

where, according to the specifications of the Challenge [1], a typical sample contains 50% of isomer I, 47 % of isomer II and 3 % of isomer III.

This Challenge was pursued here by molecular modeling and simulation, specifically, by devising effective force fields for the aqueous glycol ether mixture and calculating LLE directly by

*Corresponding author
Email address: dirk.reith@scai.fraunhofer.de (Dirk Reith)

molecular dynamics (MD). For water, the TIP4P/2005 force field by Abascal and Vega [2] was employed.

From the perspective of molecular modeling and simulation, this Challenge is rather difficult. First, the calculation of LLE is usually much more demanding than the calculation of vapor–liquid equilibria, which were in the predominant focus in the preceding challenges. Using the Gibbs Ensemble Monte Carlo (GEMC) method [3], the molecule transfer in to and out of *both* phases requires substantial computational effort. This is particularly grave for aqueous solutions, which are very dense phases with strongly interacting molecules, and also for lengthy chain-like molecules such as the glycol ethers regarded here. Second, the studied system contains four components when the three DPGDME isomers are individually resolved. Furthermore, if all stereoisomers are considered as well, the studied system contains a total of 11 molecular species. Thus, despite the fact that Monte Carlo-based methods are recommended for LLE [4], in the case of GEMC-like methods, the chemical equilibrium between the coexisting phases can only be achieved by a proper sampling of the molecular transfer for all 11 species.

Due to these intricacies, a straightforward route was chosen in the present work. The coexisting liquid phases were simulated in direct physical contact with each other by MD, hoping that the sampled time span would be sufficiently long to achieve chemical equilibrium by mutual diffusion. Another problem of this type of simulation is that the volume contains two fluid interfaces, where the composition undergoes a transition between the phases over a length scale that is non-negligible in comparison to the whole system size. Both issues can, in principle, be overcome by brute computational force, i.e. by sampling a large system over an extended period of time. Whether both issues were overcome in the calculations described below is, unfortunately, not fully clear.

Assuming proper sampling, the thermodynamic properties are fully determined by the molecular interactions. For water, the rigid four-site model TIP4P/2005 from the literature [2] was selected, because of its accurate description of the saturated liquid density and the transport properties in the liquid state [2, 5]. It is a reparameterization of the TIP4P model [9], however, it matches significantly better with the respective experimental data. In the case of the specific glycol ether species, no custom-made force fields were available. For this type of molecule, both the intermolecular and the intramolecular interactions are crucial. Stubbs et al. [10] published transferable united-atom parameter sets (TraPPE) for both interaction types to model glycol ethers, which were taken as a starting point in the present work.

To optimize the intermolecular force field parameters of DPGDME, the stand-alone software module GROW [6–8] was used. GROW is a gradient-based numerical optimization workflow that includes various efficient optimization algorithms, analysis scripts and I/O-handling that automatically invokes molecular simulation runs. Its algorithmic core is a gradient-based minimization of a quadratic loss function. This loss function compares user-defined thermo-physical properties from simulation with experimental data. Specifically, the minimization methods implemented in GROW to find optimal parameters are Steepest Descent, Newton, Conjugate Gradient and Trust Region.

2. Methodology

The intra- and intermolecular parameters of the force field for DPGDME were optimized in subsequent steps: First, the intramolecular interactions were studied for a range of different ethers by means of quantum mechanical calculations to identify their parameters. Second, the parameters of the intermolecular interactions were optimized to the experimental liquid

Table 1: United atom type, bond, angle and torsion parameters developed for 1,2-dimethoxyethane, dipropylene glycol dimethyl ether isomers and training molecules. Atom types are defined as C1: sp^3 carbon atom united with one hydrogen atom, C2: sp^3 carbon atom united with two hydrogen atoms, C3: sp^3 carbon atom united with three hydrogen atoms and OS: oxygen atom for esters.

Bond	K_l (kJ·mol^{-1}·nm^{-2})	l_o (Å)		Training Molecule
C1-C2	2300	1.52		1,2-dimethoxypropane
C1-C3	2200	1.51		1,2-dimethoxypropane
C2-C2	2400	1.53		butane
C2-C3	2400	1.51		butane
C1-OS	2500	1.41		2-methoxypropane
C2-OS	3000	1.42		2-methoxyethane
C3-OS	3500	1.41		2-methoxyethane
Angle	K_θ (kJ·mol^{-1}·rad^{-2})	θ_o (°)		Training Molecule
C2-C1-C3	700	116.5		1,2-dimethoxypropane
C2-C1-OS	800	104.0		1,2-dimethoxypropane
C3-C1-OS	900	107.0		1,2-dimethoxypropane
C3-C1-C3	800	114.0		1-methoxy-2-methylpropane
C1-C2-C3	800	112.0		ethoxybutane
C2-C2-C2	800	115.0		pentane
C2-C2-C3	800	112.0		butane
C3-C2-C3	800	112.0		propane
C1-C2-OS	900	105.0		1,2-dimethoxypropane
C2-C2-OS	900	108.0		methoxypropane
C3-C2-OS	900	108.0		methoxyethane
C1-OS-C1	950	112.0		2-(propane-2-yloxy)propane
C1-OS-C2	950	112.0		2-ethoxypropane
C1-OS-C3	950	112.0		2-methoxypropane
C2-OS-C2	950	110.5		ethoxyethane
C2-OS-C3	950	110.5		methoxyethane
Torsion	V_1 (kJ·mol^{-1})	V_2 (kJ·mol^{-1})	V_3 (kJ·mol^{-1})	Training Molecule
C3-C1-C2-C3	-11.0	-4.0	5.0	2-methylbutane, ethoxybutane
C3-C1-C2-OS	-5.6	0.0	4.8	1-ethoxy-2-methylpropane
OS-C1-C2-C3	-5.5	-5.1	0.0	ethoxybutane
OS-C1-C2-OS	-5.0	0.0	1.0	1,2-dimethoxypropane
C2-C2-C2-C3	-7.2	-3.5	6.0	pentane
C3-C2-C2-C3	-9.7	-3.4	6.3	butane
C3-C2-C2-OS	-0.0	0.0	6.0	methoxypropane
OS-C2-C2-OS	-1.0	4.9	6.0	1,2-dimethoxyethane
C2-C1-OS-C1	-24.0	-7.0	0.0	2-(propane-2-yloxy)butane
C2-C1-OS-C2	-25.0	-11.0	5.0	ethoxybutane
C2-C1-OS-C3	-23.0	-10.3	0.0	1,2-dimethoxypropane
C3-C1-OS-C1	-25.0	-7.0	3.0	2-(propane-2-yloxy)butane
C3-C1-OS-C2	-30.0	-14.0	2.0	ethoxybutane
C1-C2-OS-C1	-7.1	0.0	5.0	dipropylene glycol dimethyl ether
C1-C2-OS-C2	-26.1	-7.0	4.0	1-ethoxy-2-methylpropane
C1-C2-OS-C3	-30.7	-9.6	4.0	1,2-dimethoxypropane
C2-C2-OS-C2	-27.0	-8.0	4.0	1-ethoxypropane
C2-C2-OS-C3	-29.0	-8.0	3.8	1,2-dimethoxyethane
C3-C2-OS-C1	-16.8	-6.5	2.0	ethoxybutane
C3-C2-OS-C2	-29.0	-9.4	4.1	ethoxyethane
C3-C2-OS-C3	-29.8	-8.3	4.5	methoxyethane
Improper Torsion	V_2 (kJ·mol^{-1})	Lennard–Jones	σ (Å)	ϵ (K)
C3-C3-C1-C2	60.0	C1	4.3300	10.00
C3-C3-C1-OS	60.0	C2	3.9501	46.00
		C3	3.7310	98.00
		OS	2.8039	55.01

density of 1,2-dimethoxyethane (CH_3-O-CH_2-CH_2-O-CH_3). Third, all parameters were transferred to DPGDME. The intermediate step was taken because experimental LLE data for the 1,2-dimethoxyethane/water mixture are available in the considered temperature range for validation.

2.1. Intramolecular Parameters

All molecules listed in Table 1 were optimized using the HF/6-31G(d)//HF/6-31G(d) theory level, providing reliable target geometry data for intramolecular parameter development. B3LYP/6-311++G(2d,2p)//HF/6-31G(d) single-point calculations were performed to obtain more reliable target energetics data for parameter fitting [12]. The accuracy and use of these theories has been discussed previously [12, 13]. A 49 Å distance was used to generate the short-range neighbor list, as well as for the cutoff distance for nonbonded and electrostatic interactions. This distance encompasses the molecular diameter of every molecule studied. The 1–4 nonbonded and electrostatic scaling factors were set to unity [13]. Partial atomic charges and Lennard–Jones parameters were assigned according to those of the united-atom TraPPE force field [10].

The parameters were developed using the GROMACS force field equation [14]. All torsion parameters were initially derived using the fitting algorithm in Gnuplot [15], by optimizing all possible combinations of the V_1, V_2 and V_3 terms. The phase angles were constrained to zero, since they are unnecessary for fitting torsion profiles. The parameters that best represent our chemical intuition (e.g. V_2 terms for rotation about double bonds) were chosen for further optimization. This was manually and iteratively done, allowing specific conformations (e.g. transition states or minima) to preferentially be weighted.

Angle parameters were optimized by defining a new bond between the first and third atom of the investigated bending and then constraining that distance to the value optimized in the HF calculations. During angle parameter optimizations, all bonds were constrained using the linear constraint solver (LINCS) algorithm. Dihedral restraints used the default restraint equation in GROMACS. Geometries were optimized using a Conjugate Gradient algorithm until the force convergence tolerance of 0.01 $\mathrm{kJ{\cdot}mol^{-1}{\cdot}nm^{-1}}$ was obtained. Unlike Lennard–Jones parameters between the ether molecules were determined by the Lorentz–Berthelot combination rule.

2.2. Molecular Dynamics

The same settings stated above were used in all present MD calculations. Particle Mesh Ewald summation was employed for calculating the electrostatic energy beyond a 9 Å cutoff radius [16, 17]. All bonds were constrained to their l_o length shown in Table 1 using the LINCS algorithm, and subsequent force evaluations were computed without these bonds. Temperature control was achieved using the Nosé-Hoover thermostat and the Rahman-Parrinello barostat with coupling times $\tau_\mathrm{T} = 0.5$ ps and $\tau_\mathrm{P} = 2.0$ ps, respectively. Condensed-phase simulations were performed using periodic boundary conditions at a constant pressure of 1 bar.

The GAMESS [18, 19] program was used to perform the quantum mechanical calculations. The GROMACS [14] program was employed for all molecular mechanics and dynamics calculations.

2.3. Intermolecular Parameters

The Lennard–Jones parameters σ and ϵ for all atomic groups were determined by GROW [6, 7]. The experimental target data used for optimization here was the liquid density $\rho(T)$ of 1,2-dimethoxyethane as a function of the temperature T in a pre-defined temperature range $\mathcal{T}$ at

1 bar. Only the liquid density was chosen because no other convenient experimental data were available. For other available properties, like diffusion coefficient or shear viscosity, the required simulation time would have been too long within the framework of the Challenge. The following *loss function* was minimized with respect to a set of Lennard–Jones parameters $\boldsymbol{x}$:

$$F(\boldsymbol{x}) := \sum_{T \in \mathcal{T}} w_{\rho(T)} \left(\frac{\rho^{\mathrm{exp}}(T) - \rho^{\mathrm{sim}}(\boldsymbol{x}, T)}{\rho^{\mathrm{exp}}(T)} \right)^2, \tag{1}$$

where $\rho^{\mathrm{exp}}(T)$ is the experimental and $\rho^{\mathrm{sim}}(\boldsymbol{x}, T)$ the simulated liquid density. The weights $w_{\rho(T)}$ account for the fact that due to statistical noise in both experimental and simulated data, some of the properties may be more accurate than others. However, all density values were treated equally here, i.e. $w_{\rho(T)} \equiv const.$

The main advantage of gradient-based algorithms, besides their fast convergency, is the fact that they are always directed to the minimum because of the use of descent directions. This means that they do not stray within the parameter space, which would lead to unnecessary function evaluations. Please note that each function evaluation within the optimization procedure requires time-consuming molecular simulation runs, and it is advantageous to keep these low in number.

A drawback of such methods is that they are only locally convergent, i.e. they require an initial parameter vector that is not too far away from a local minimum. Moreover, an admissible domain for the force field parameters has to be defined, in which the minimum should be situated. Therefore, a function-adapted step length control was applied so that the optimization algorithm does not lead out of the domain. This was done by the Armijo step length control (see e.g. [20]) because it does not require too many additional simulations.

The initial force field parameters were taken from the TraPPE force field [10], as they claim transferability and accuracy over a wide temperature range. The admissible domain for the force field parameters was determined in the following way: The size parameter σ was not changed by more than 30% and the energy parameter ϵ was not changed by more than 40%. A stopping criterion for the optimization procedure was *a priori* not defined. The quality of the resulting force field was determined from the deviation of the simulated liquid density from the experimental data.

The optimization method applied in this work was a Conjugate Gradient method, namely the Polak–Ribière algorithm (see e.g. [20]). Conjugate Gradient methods combine two successive gradients and descent directions by the iteration procedure

$$\boldsymbol{d}^{k+1} = -\nabla F(\boldsymbol{x}^{k+1}) + \alpha_k \boldsymbol{d}^k, \;\; k = 0, 1, 2, ..., \tag{2}$$

where $\boldsymbol{d}^0 = -\nabla F(\boldsymbol{x}^0)$. The parameter α_k was determined by the following combination of the gradients

$$\alpha_k = \frac{\langle F(\boldsymbol{x}^{k+1}) - F(\boldsymbol{x}^k), F(\boldsymbol{x}^{k+1}) \rangle}{||F(\boldsymbol{x}^k)||^2}. \tag{3}$$

After a systematic testing, the Polak–Ribière method turned out to be one of the fastest and most robust optimization methods used [8]. Furthermore, it is one of the few methods which get very close to the minimum despite the presence of statistical noise.

Table 2: Liquid density of 1,2-dimethoxyethane at 1 bar from present simulations compared to experimental data [21].

T	exp.	sim. (Stubbs et al.)	deviation	sim. (this work)	deviation
K	kg m^{-3}	kg m^{-3}	%	kg m^{-3}	%
283	876.9	875.2	-0.19	887.7	1.24
293	866.5	862.6	-0.45	875.5	1.02
303	855.1	850.7	-0.51	862.9	0.90
343	809.5	800.3	-1.14	811.1	0.19
353	798.1	787.4	-1.34	796.8	0.16

3. Parameterization of 1,2-Dimethoxyethane and Liquid–Liquid Equilibria with Water

3.1. Force Field Parameterization

The liquid density of 1,2-dimethoxyethane on the basis of the force field of Stubbs et al. [10] deviates from the experimental data by about 1%, cf. Figure 1. In order to test whether this force field can reproduce the molecular conformations as well, it was evaluated against quantum mechanically calculated bending and angle potentials. As an example, the torsion energy profile of the O-C-C-O dihedral angle is shown in Figure 2. Because of the obviously large deviations between the quantum mechanical data and the results obtained on the basis of the TraPPE force field by Stubbs et al., the intramolecular force field was completely reparameterized. As can be seen in Figure 2, the reparameterization improved the agreement between the resulting molecular mechanics and quantum mechanics rotational profile. Of particular importance is the improved agreement seen for the two minima and rotational barriers. The new intramolecular force field, combined with the TraPPE intermolecular parameters, leads to somewhat larger deviations from the experimental data (Figure 1). This shows the influence of the molecular conformation on the liquid density. Thus, a reparameterization of the intermolecular parameters was necessary.

1,2-dimethoxyethane consists of three different molecular groups, i.e. methyl (C3), methylene (C2) and oxygen (OS), which were all considered within the GROW optimization procedure. This resulted in a six-dimensional optimization problem for σ(C3), σ(C2), σ(OS), ϵ(C3), ϵ(C2) and ϵ(OS). The experimental liquid density by Zheng et al. [21] in the temperature range from 273 to 373 K was taken as a target for fitting the Lennard–Jones parameters.

The results of the optimization by GROW are summarized in Figure 1 and Table 2. Within one iteration, the gradient-based optimization method found significantly better Lennard–Jones parameters for the liquid density. Using the new force field, the liquid density only deviates from the experiment in most cases by less than 1%, except for 283 K. The combined force field (present intramolecular parameters and intermolecular parameters by Stubbs et al. [10]) is a little worse than the one provided by [10] due to the different intramolecular parameters. However, the present force field with optimized intermolecular parameters yields a liquid density with a quality that is similar to the model by Stubbs et al. After the second iteration, the Armijo step length control did not find a lower loss function value after ten iterations, i.e. a reasonable amount of computation time. Therefore, GROW was terminated at this point so that the parameters of the second iteration were considered as the final values.

As shown by Figure 1, the slope of the temperature dependence of the liquid density could not

Table 3: LLE of the 1,2-dimethoxyethane/water mixture at 333 K and 1 bar from present simulations compared to experimental data [22].

phase	exp. ether mol%	sim. ether mol%	deviation mol%	exp. water mol%	sim. water mol%	deviation mol%
ether	72.4	73.6	1.2	27.6	26.4	-1.2
water	9.0	9.9	0.9	91.0	90.1	-0.9

Table 4: Liquid density of DPGDME at 1 bar from present simulations compared to experimental data [23].

T / K	exp. kg m^{-3}	sim. (Stubbs et al.) kg m^{-3}	deviation %	sim. (this work) kg m^{-3}	deviation %
283	913.0	888.3	-2.7	903.5	-1.0
303	894.0	866.5	-3.1	880.8	-1.5
323	875.4	–	–	858.6	-1.9
353	846.9	815.8	-3.7	826.9	-2.4

be reproduced exactly. A change in the intermolecular force field parameters could only shift the curve upwards but could not alter its slope.

3.2. Liquid–Liquid Equilibria of the 1,2-Dimethoxyethane/Water Mixture

The performance of the new force field was additionally tested with respect to the LLE of the 1,2-dimethoxyethane/water mixture (Figure 3). To do this, a simulation volume with two phases at a composition equal to the experimental values [22] was generated. This volume was equilibrated for 4 ns at 333 K and subsequently sampled over 1 ns. The Lorentz–Berthelot combining rules were employed for the unlike intermolecular interactions. The small deviations (Table 3) in both the water and the ether phase led to the conclusion that the present ether force field was compatible with the TIP4P/2005 water force field and no further parameterization was needed.

4. Parameterization of Dipropylene Glycol Dimethyl Ether and Liquid–Liquid Equilibria with Water

4.1. Force Field Parameterization

The Lennard–Jones parameters were directly transferred from 1,2-dimethoxyethane to the force field for DPGDME. Additionally, the C1 atom type was introduded with the TraPPE parameters. The resulting force field was tested against the experimental liquid density from Esteve et al. [23], cf. Figure 4. The new DPGDME force field shows a deviation from experimental liquid density data that is roughly half of that determined on the basis of the force field by Stubbs et al., cf. Table 4.

4.1.1. Liquid–Liquid Equilibria of the Dipropylene Glycol Dimethyl Ether/Water Mixture

Production runs for the Challenge were performed using the new DPGDME force field. To determine the optimal size of the simulation volume and to obtain a first estimate of the initial partial densities, preliminary simulations were executed. Thereby, volume dimensions of ca. 37 nm $\times$ 9 nm $\times$ 9 nm were chosen. The length of the volume in x direction was chosen to be about four times larger than in the other two directions. This realized a good ratio between

Table 5: LLE of the DPGDME/water mixture at 1 bar.

	DPGDME in DPGDME			DPGDME in water			water in DPGDME			water in water		
T	ρ_D	x_D	Std.	ρ_D	x_D	Std.	ρ_W	x_W	Std.	ρ_W	x_W	Std.
K	kg m^{-3}	mol%	mol%	kg m^{-3}	mol%	mol%	kg m^{-3}	mol%	mol%	kg m^{-3}	mol%	mol%
283	938.0	65.9	5.2	254.0	3.2	0.3	54.0	34.1	2.7	836.2	96.8	7.8
323	913.9	67.5	5.4	108.4	1.6	0.2	49.1	32.5	2.6	864.7	98.4	8.0
333	900.0	67.1	5.3	86.2	1.2	0.2	48.1	32.9	2.6	932.7	98.8	8.1
353	895.6	67.9	5.5	65.7	0.4	0.1	46.7	32.1	2.5	926.4	99.6	8.2

phase size and interphase area. Because of the required volume dimension, the system contained 47503 water and 6134 DGPDME molecules.

Since the DPGDME molecule exhibits two chiral centers, additional stereoisomers exist for each of the three isomers. There are three, four and three stereoisomers for isomer I, II and III, respectively. Due to the fact that the liquid density of DPGDME depends on the conformational space and the packing of the molecules in the condensed phase, it was decided to consider all stereoisomers in the simulation. Thus, the total number of DPGDME molecules was distributed to all ten stereoisomers accordingly.

For each temperature, the system was equilibrated over 5 ns at constant temperature and pressure. The subsequent production run was sampled for another 5 ns. The resulting partial density profiles for 283 and 353 K are shown in Figure 5. The partial densities in the water phase were averaged over an interval between 2 and 12 nm and in the DPGDME phase they were averaged over an interval between 22 and 31 nm to determine the data required for the Challenge. For reasons of statistical analysis, a snapshot was recorded every 50ps.

Molar fractions of 44.3 mol% DPGDME in the DPGDME phase and 0.3 mol% DPGDME in the water phase were chosen as a initial guess. These data are far off the experimental values from Dow Chemical [24], where 70.2 and 5.7 mol% for DPGDME in DPGDME and DPGDME in water at 298 K are indicated, respectively. However, we deemed it to be important to test how stable the phases behave under more favorable conditions before choosing a more realistic solubility starting point for the Challenge production runs. From these simulations we observed that the phases were indeed stable and showed the experimentally correct trends in solubility behaviour. In terms of absolute values, the resulting molar fraction in the water phase (0.3 mol% at 283 K) was too small in comparison to the experimental one (5.7 mol% at 298 K).

Thus, it was decided to proceed to better starting concentrations with one large phase (to enhance the slab width and, thus, the quality of the measurement) and one small phase both for DPGDME and for waterp phase, respectively. More specifically, we first simulated the water phase for all temperatures starting at the experimental molar fractions (only available at 298 K). In these simulations, only a small DPGDME phase, consisting of 200 DPGDME molecules, was introduced to enable the system to equilibrate. Thereby, volume dimensions of ca. 25 nm $\times$ 6 nm $\times$ 6 nm and system sizes containing 30000 water and 875 DPGDME molecules were selected. The equilibration run was sampled over 5 ns and the production run over 2 ns. We then simulated the DPGDME phase for all temperatures also starting at the experimental molar fraction at 298 K. Here again a volume of ca. 37 nm $\times$ 9 nm $\times$ 9 nm containing 47503 water and 6134 DGPDME molecules was prepared. The equilibration and production runs took both 5 ns. The resulting partial densities are shown in Figure 6.

5. Results

The partial density profiles in Figure 5 exhibit a very interesting shape. In the water phase large DPGDME domains are forming. That is why it was necessary as dicussed before to simulate a larger water phase. The interphase between water and DPGDME was dominated by a membrane-like region, where water was almost absent. The molar fraction of DPGDME shows a weak temperature dependence in these simulations (Table 5 and Figures 7 and 8).

The molar fraction of DPGDME in the water phase is more temperature dependent (Table 5 and Figures 7 and 8). With increasing temperature, the molar fraction is decreasing.

Our results for the Challenge, i.e. the LLE data for the DPGDME/water mixture obtained by our methodology and simulations, are summarized in Table 5. Please note that smoothed values were taken from a linear fit to the simulation data, cf. Figures 7 and 8.

6. Conclusion

In the context of the Sixth Industrial Fluid Property Simulation Challenge (IFPSC) 2010, the LLE of the DPGDME/water mixture was studied at 283, 323, 333 and 353 K and 1 bar. For water, the TIP4P/2005 force field was used and for DPGDME a new force field was developed, considering all ten relevant stereoisomers. For the parmetrization of the ethers, specific methodologies were employed: The bending and torsion potential profiles of ethers were determined by quantum mechanical calculations. Dihedral and bond angle constants were fitted to these energy profiles. Throughout, classical MD simulations with the GROMACS force field equation were performed. The charge magnitudes were taken from the TraPPE force field, and the Lennard–Jones parameters were optimized to experimental liquid density data of 1,2-dimethoxyethane using the gradient–based optimization workflow GROW. For the 1,2-dimethoxyethane/water mixture, experimental LLE data are available in the temperature range of interest. Hence, the performance of the force field could favorably be assessed for that mixture. The new force field parameters were directly transferred to DPGDME, which turned out to better perform than the TraPPE force field with respect to the liquid density.

The equilibration and production runs at the four different temperatures 283, 323, 333 and 353 K of the DPGDME/water mixture were executed in periodic simulation volumes, each containing two bulk phases and an interface region. It turned out that the temperature dependence of the molar fraction of DPGDME in water is stronger than that of water in DGPDME. In the water phase, the molar fraction of DPGDME decreased with increasing temperature. In the DPGDME phase, the molar fraction of water increased with increasing temperature. Our entry to the Challenge is given in Table 5.

7. Acknowledgements

We are grateful to the *Kölsches Grundgesetz*, Article 3: *"Et hätt noch immer jot jejange."*

References

[1] The Sixth Industrial Fluid Properties Simulation Challenge (IFPSC), `http://www.ifpsc.org`.

[2] J. L. F. Abascal, C. Vega, J. Chem. Phys. 123 (2005) 234505.

[3] A. Panagiotopoulos, Mol. Phys. 61 (1987) 813–826.

[4] D. N. Theodorou, Ind. Eng. Chem. Res. 49 (2010) 3047–3058.

[5] G. Guevara-Carrion, J. Vrabec, H. Hasse, J. Chem. Phys. (2010) submitted.

[6] M. Hülsmann, T. Köddermann, J. Vrabec, D. Reith, Comput. Phys. Commun. 181 (2010) 499–513.

[7] M. Hülsmann, T. J. Müller, T. Köddermann, D. Reith, Mol. Sim. (2010) accepted.

[8] M. Hülsmann, J. Vrabec, A. Maaß, D. Reith, Comput. Phys. Commun. 181 (2010) 887–905.

[9] W. L. Jorgensen, J. Chandrasekhar, J. D. Madura, R. W. Impey, M. L. Klein, J. Chem. Phys. 79 (1983) 926–935.

[10] J. M. Stubbs, J. J. Potoff, J. I. Siepmann, J. Phys. Chem. B 108 (2004) 17596–17605.

[11] Y. Gil, E. Deelman, M. Ellisman, T. F. Fahringer, G. Fox, D. Gannon, C. Goble, M. Livny, L. Moreau, J. Myers, Computer 40 (2007) 24–32.

[12] J. H. Lii, B. Y. Ma, N. L. Allinger, J. Comp. Chem. 20 (1999) 1593–1603.

[13] K. N. Kirschner, A. B. Yongye, S.M. Tschampel, J. Gonzalez-Outeirino, C. R. Daniels, B. L. Foley, R. J. Woods, J. Comp. Chem. 29 (2008) 622–655.

[14] B. Hess, C. Kutzner, D. van der Spool, E. Lindahl, J. Chem. Theory Comput. 4 (2008) 435–447.

[15] H. B. Broeker, J. Campbell, R. Cunningham, D. Denholm, G. Elber, R. Fearick, C. Grammes, L. Hart, L. Hecking, T. Koenig, D. Kotz, E. Kubaitis, R. Lang, A. Lehmann, A. Mai, C. Steger, W. J. van der Tom Tkacik, J. R. van Zandt, A. Woo, E. Merritt, P. Mikulýk, J. Zellner, Gnuplot version 4.2, patchlevel 3, 2007.

[16] T. Darden, D. York, L. Pedersen, J. Chem. Phys. 98 (1993) 10089–10092.

[17] U. Essmann, L. Perera, M. L. Berkowitz, T. Darden, H. Lee, L. G. Pedersen, J. Chem. Phys. 103 (1995) 8577–8593.

[18] W. M. Schmidt, K. K. Baldridge, A. J. Boatz, T. S. Elbert, S. M. Gordon, H. J. Jensen, S. Koseki, N. Matsunaga, A. K. Nguyen, S. Su, L. T. Windus, M. Dupuis, A. J. Montgomery, J. Comp. Chem. 14 (1993) 1347–1363.

[19] M. S. Gordon, M. W. Schmidt, in: M. S. Gordon, M. W. Schmidt, C. E. Dykstra (Eds.), Theory and Applications of Computational Chemistry: the First Forty Years, Elsevier, Amsterdam, Boston, 2005, pp. 1167–1189.

[20] J. Nocedal, S. J. Wright, Numerical Optimization, Springer, New York, 1999.

[21] P. Zheng, X. Meng, J. Wu, Z. Liu, Int. J. Thermophys. 29 (2008) 1244–1256.

[22] G. J. Pierotti, C. H. Deal, E. L. Derr, Ind. Eng. Chem. 51 (1959) 95–102.

[23] X. Esteve, A. Conesa, A. Coronas, J. Chem. Eng. Data 48 (2003) 392–397.

[24] Dow Chemical, `www.dow.com`.

List of Figures

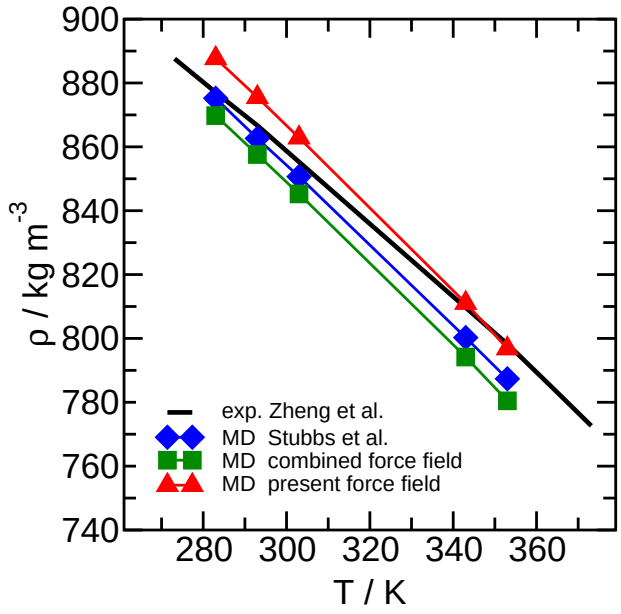

Figure 1:

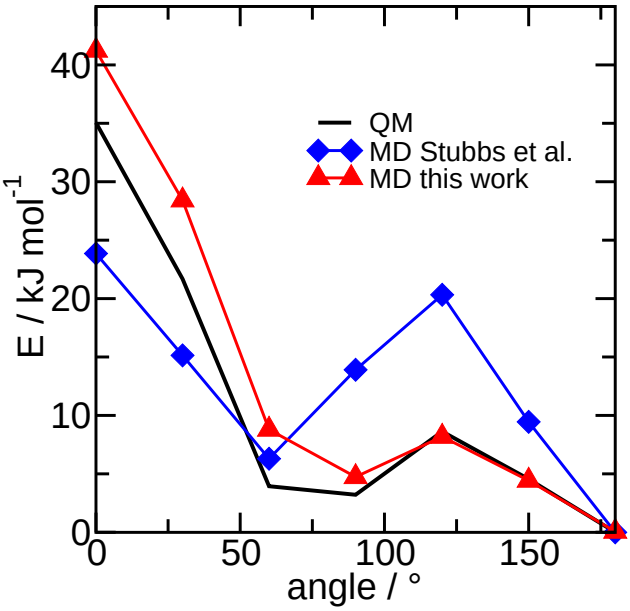

Figure 2:

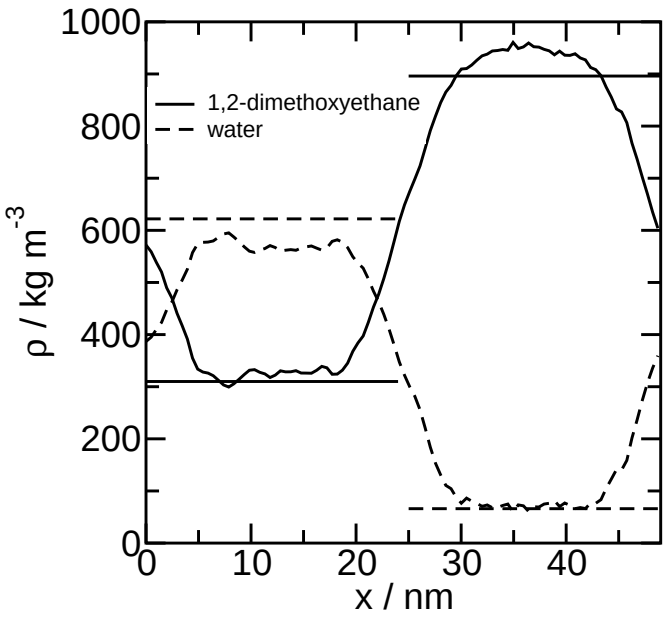

Figure 3:

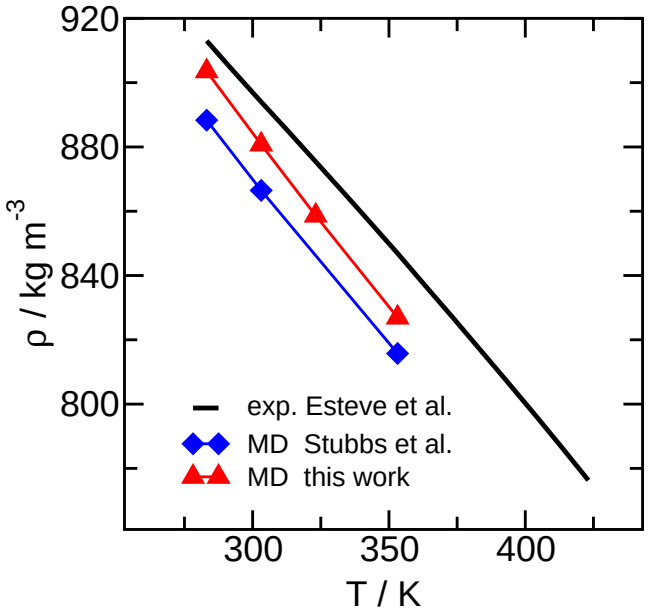

Figure 4:

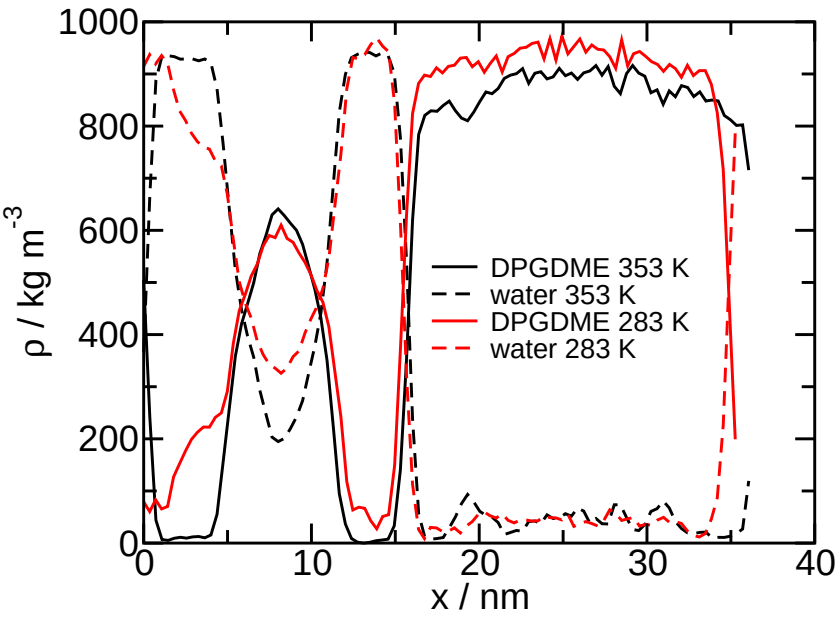

Figure 5:

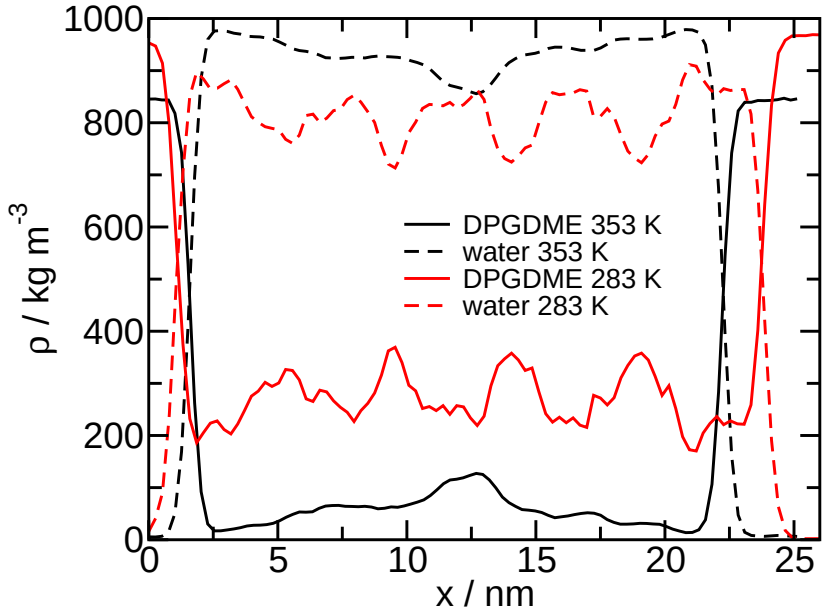

Figure 6:

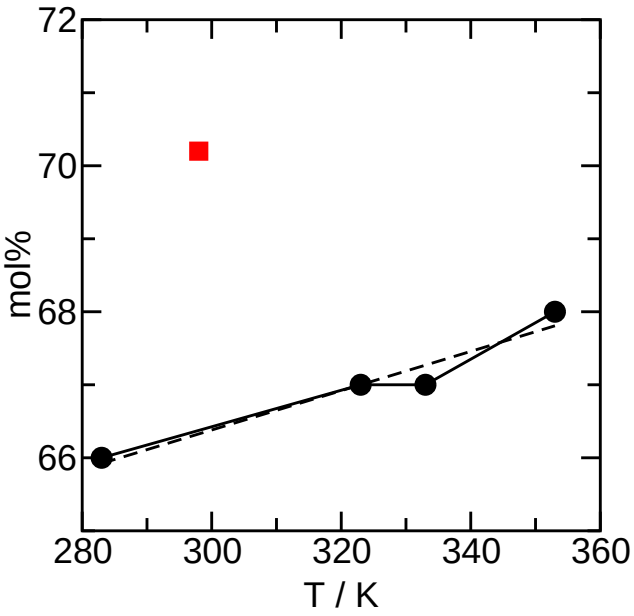

Figure 7:

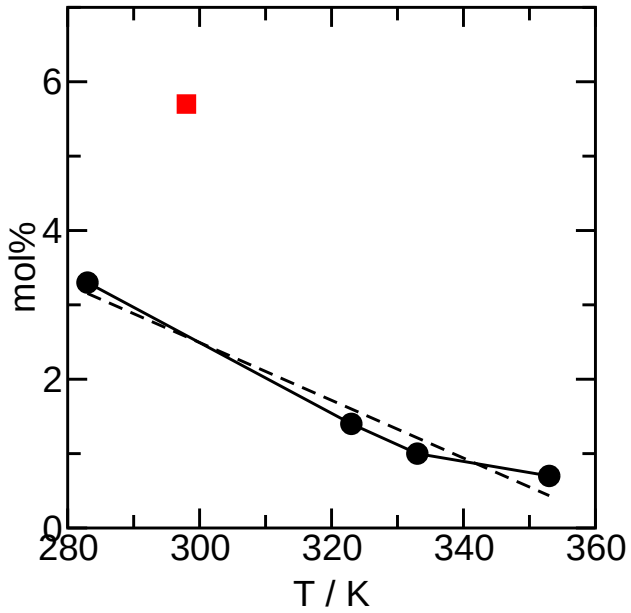

Figure 8: